CHAPTER 55

WAVE CLIMATE ASSESSMENT IN THE SOUTH AEGEAN SHELF

Spiros Christopoulos [1], Christos Solomonidis[2]

Abstract

Wave climate parameters are estimated in a coastal area in the South Aegean Sea with the use of wave hindcast, wave transformation and spectral transformation models. The relative performance of these models is judged with the aid of a field measurements campaign. It is shown that most models can give the correct prediction in the intermediate depth waters, whereas only models taking into account nonlinear phenomena can match the measurements in the very shallow water area.

Intoduction

The correct estimation of the wave climate parameters such as wave height and period both in deep waters and in the coastal zone, is of paramount importance for the design of offshore and coastal works, safe navigation and the operation of marine systems such as fisheries.

For the determination of the wave conditions in deep and intermediate depth waters, a series of hindcast models have been developed and validated by many researchers. Second generation hindcast models are already used by various meteorological centres, as is the UK Met. Office, for daily prediction of the wave conditions, usually updated every 6 hours. Even third generation hindcast models, like the WAM, are used for hindcasts in European waters. The use of third generation models for operational purposes has been explored extensively (Komen et al., 1994).

Numerical models for wave transformation in the nearshore area have been used for many years for research and for coastal engineering design purposes as well. A large number of monochromatic wave models, based either on Berkoff's Mild Slope Equation (Berkhoff, 1976) or on geometrical physics (ray tracing) are widely used in applications. Spectral models based

1) Dr. Eng., Aristotle University of Thessaloniki, Department of Civil Engineering, Division of Hydraulics & Environmental Engineering, 540 06 Thessaloniki, Greece.

2) Dr. Eng., Marine Technology Development Company S.A., 2nd Merarchias 16, 185 35 Piraeus, Greece.

on the energy balance equation are also used, whereas spectral models, which solve Boussineq type equations, including non-linear energy dissipation processes (Madsen et al., 1991) are gaining popularity recently. Research is under way for the refinement of these models in order to include the non-linear interaction of spectral ordinates (Komen et al., 1994).

Despite the variety of numerical wave models, not much work has been done for their calibration with simultaneous wave measurements, and even less in the direction of assimilating the measurements in the models themselves. The recent abundance of satellite imagery is facilitating though this task.

In the work which is presented in this paper, the wave climate in an area of the South Aegean Sea (North Coast of Crete), is assessed with the aid of wave hindcast and numerical wave transformation models as well as semi- analytical (spectral transformation) methods, in conjuction with in situ wave measurements.

Wave Measurements

A field campaign of wave measurements was conducted in the context of MAST2-WAVEMOD project at a site near Rethymno, in the North coast of Crete, Greece. The field campaign was conducted by the French Insitute IFREMER, subcontracting to METEOMER, with the collaboration of MARTEDEC and the Institute of Marine Biology of Crete. Two directional and one non-directional wave riders (all by Datawell) were used for the wave measurements, deployed along the predominant direction of wave attack, at three locations of different depths (100m and 10m for the directional waveriders, 20m for the non-directional). The campaign lasted for a period of 10 months, in particular from the 1st of February to the 28th Novenber 1994. Next to each waverider, a current meter was deployed; two AANDERA RCM 7 were used at the 100 and 20 m locations, and a S4DW current and wave measuring instrument, by InterOcean, was used at the 10 m location (Solomonidis 1995, Paillard 1995).

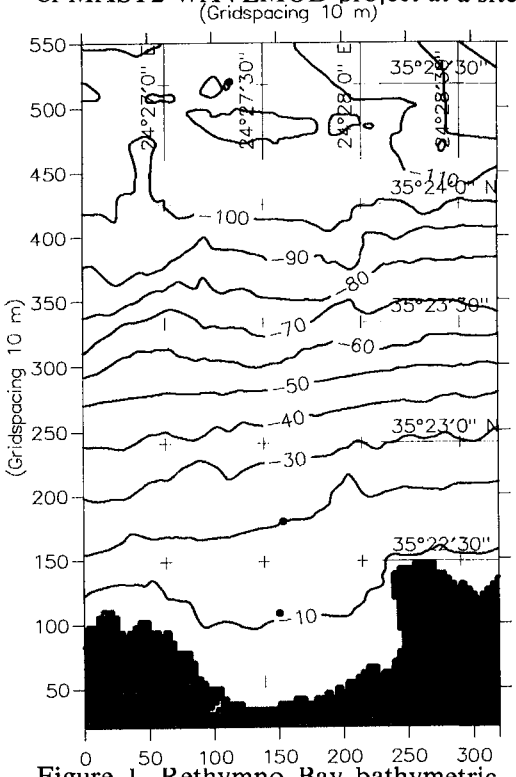

Figure 1. Rethymno Bay bathymetric grid and locations of the wave riders

At the same time, a fully equiped land based station was installed in a public building and overlooking the area of the experiment. The raw data (timeseries of heave and N-S & E-W translation), as well as spectral data processed on board the wave riders, were continuously transmitted via VHF to the land based station. The sampling rate for the directional buoys was 1.28 Hz, recording for 20 min every 30 min, and 2.56 Hz for the non-directional buoy, recording for 20 min every 20 min. The bathymetry of the area as well as the locations of the instruments is shown in Figure 1.

Intense climatic incidences were recorded during February (11-13), March (5-6, 10-14), October (10-16) and November (15-16, 20-24), with significant wave heights Hs from 3 - 6 m, peak periods Tp from 9 to 10 sec and predominant directions North to North West. In Figure 2 the significant wave heights Hs recorded at the location of the offshore buoy are shown.

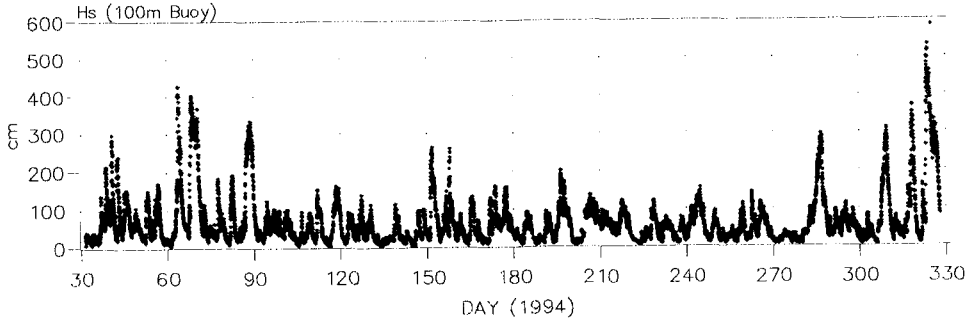

Figure 2. Time history of H_s from the 100m wave rider.

Wave Hindcast Model

The wave climate in the broader area is assessed with the aid of a second generation wave model (Christopoulos & Koutitas, 1991). The model AUT simulates the wave energy balance equation, which for deep water is written as

$$\frac{\partial F}{\partial t} + c_g \cos\theta \frac{\partial F}{\partial x} + c_g \sin\theta \frac{\partial F}{\partial y} = S_{in} + S_{nl} + S_{ds} \qquad (1)$$

where $F(f,\theta;x,y;t)$ is the spectral energy density of the wave component (f,θ) at location (x,y) and time t, c_g the group velocity, S_{in} the wind input, S_{nl} the nonlinear wave energy transfer and S_{ds} the wave dissipation due to white capping.

The equation is solved using the fractional step method, where for the advection a first order upwind scheme is adopted. For the wind input the Bight of Abaco result is used, while the wave dissipation is represented by means of Komen's et al. (1984) explicit formula. The nonlinear energy transfer between the various wave components is estimated implicitly through the redistribution of the wave energy, after the above steps, according to a Jonswap spectrum having the same wave energy.

The model is implemented in the whole area of Aegean Sea with grid resolution of 1/6 of a degree. For the wind data, the ECMWF data from analysis results are used. The model output is compared with the results from

the deep buoy for the storm of March 1994 (Figure 3). As it can be seen, there is a good agreement for the characteristic wave parameters of the significant wave height and the mean wave period.

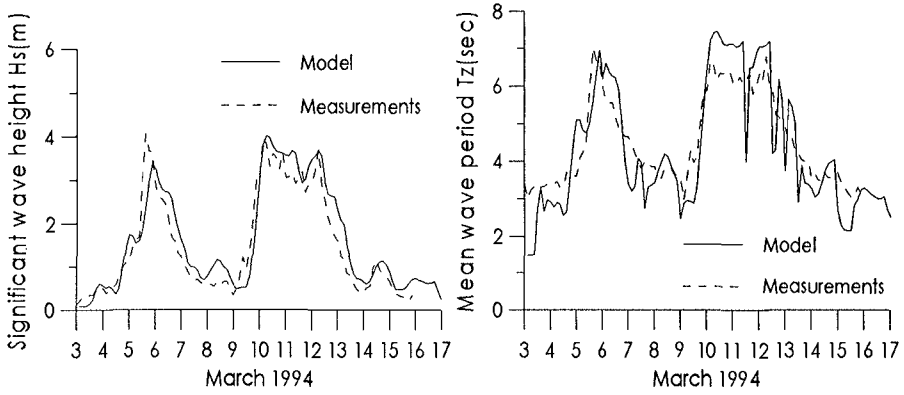

Figure 3. AUT model results for 3-17 March 1994

Numerical Wave Transformation Models

The offshore wave climate is specified either from the deep water wave hindcast model results or from the offshore wave buoy data. From the offshore location the deep water waves propagating to the coastal zone, are transformed to the shallow water waves through various physical processes like refraction, shoaling, diffraction, wave breaking, bottom friction and nonlinear energy transfer. For the simulation of these transformation processes three different numerical models are used, a shallow spectral model, an elliptic mild slope model and a Boussinesq wave model. The spectral model is a version of the AUT hindcast wave model, while the other two are belonging to DHI's suite of programs MIKE 21, namely MIKE 21 EMS (Elliptic Mild Slope) and MIKE 21 BW (Boussinesq).

The results of the models in the vicinity of the two inner buoys locations are compared with the corresponding measurements of the buoys. A short description of the numerical wave transformation models, as well as the way in which they are used in the present work, will be given in the following paragraphs.

Shallow Spectal Model

The shallow spectral model SAUT is a modified version of the AUT deep water wave model. The governing equation is

$$\frac{\partial F}{\partial t} + c_g \cos\theta \frac{\partial F}{\partial x} + c_g \sin\theta \frac{\partial F}{\partial y} + \partial\{(c_g \cdot \nabla\theta)F\} / \partial\theta = S_{bf} + S_{ds} \qquad (2)$$

where the refraction term is added on the left-hand side of the equation, while the processes of the bottom friction and wave dissipation are taken into account on the right-hand side.

The refraction term is based on Snell's law and after some manipulations is solved through

$$c_g \cdot \nabla\theta = -\frac{|c|}{k}\left(\frac{\partial H}{\partial x}sin\theta - \frac{\partial H}{\partial y}cos\theta\right)\left(\frac{-k^2 sech^2 kH}{tanhkH + kHsech^2 kH}\right) \quad (3)$$

where k is the wave number and H the water depth. For the full refraction term the upstream difference in θ is expressed in flux form with the upstream direction determined by the sign of $c_g \cdot \nabla\theta$. The resulting difference for a single component may be written (Golding, 1983)

$$[\Delta F]_\theta = -\frac{\partial}{\partial\theta}\{(c_g \cdot \nabla\theta)F\}\Delta t$$

$$= \left\{ \left[min\begin{pmatrix} c_g \cdot \nabla\theta \\ 0 \end{pmatrix} \cdot F \right]_{\theta+\Delta\theta} + \left[max\begin{pmatrix} c_g \cdot \nabla\theta \\ 0 \end{pmatrix} \cdot F \right]_{\theta-\Delta\theta} - [(c_g \cdot \nabla\theta)F]_\theta \right\} \frac{\Delta t}{\Delta\theta} \quad (4)$$

The bottom friction is calculated using the Collins formula, while the calculated wave heights are checked using the following wave breaking criterio (Battjes & Jannsen, 1978)

$$H_m = 0.88k^{-1} tanh(0.78kH / 0.88) \quad (5)$$

The model is implemented on the area of Rethymno Bay with space step of 200m and time step of 15 sec. Results for the episode of March 1994 - date 03052300 (MMDDhhmm) are shown in Figure 4.

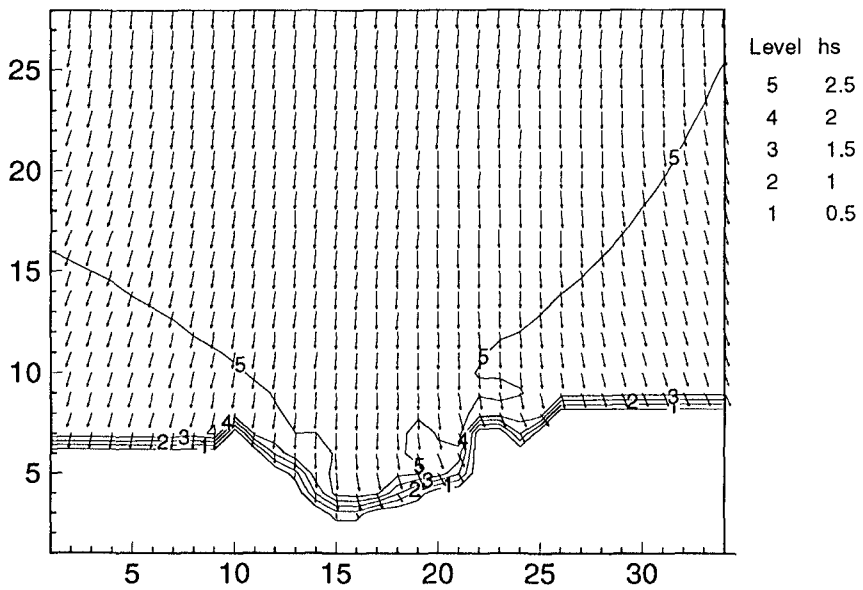

Figure 4. SAUT simulation, input H_s=2.98m, T_z=6.3sec, θ=185°

Elliptic Mild Slope Model

This program simulates the propagation of monochromatic waves over a gently sloping bathymetry. It basically solves numerically the Elliptic

Mild Slope equations (Berkhoff, 1976) which take into account the combined effects of shoaling, refraction, diffraction and back-scattering. The equations have been generalised in order to include the internal generation of waves, absorption by sponge layers, partial reflection by breakwaters or other structures, and energy dissipation due to bed friction and wave breaking.

The basic set of equations which are numerically solved in this model (MIKE 21 EMS manual) are the following:

$$\begin{aligned} &\lambda_1 \frac{\partial S}{\partial t} + \lambda_2 S + \frac{\partial P}{\partial x} + \frac{\partial Q}{\partial y} = SS \\ &\lambda_1 \frac{\partial P}{\partial t} + \lambda_3 P + c_g^2 \frac{\partial S}{\partial x} = 0 \\ &\lambda_1 \frac{\partial Q}{\partial t} + \lambda_3 Q + c_g^2 \frac{\partial S}{\partial y} = 0 \end{aligned} \qquad (6)$$

where S, P and Q are complex variables of x, y, t expressing surface elevation and flux densities (in x and y directions) respectively, SS is the source magnitude per unit horizontal area, whereas the λ coefficients are terms which include frictions due to porous structures and sponge layers, and energy dissipation effects.

These equations are solved by implicit finite difference techniques. The double sweep algorithm is utilised, which is a form of the Gauss elimination.

The bathymetric grid which was used for the model extends to the line of -50m, which is sufficient so as to be considered as deep water conditions. A number of sponge layers is introduced in order to absorb wave energy.

Two parameters in the model set-up can be used for calibration purposes. One is the *bed friction*. For Rayleigh distributed wave heights, the energy dissipation is (MIKE21 EMS manual):

$$\frac{dE}{dt} = \frac{-1}{8\pi^{1/2}} \frac{f_e/2}{g} \left(\frac{\omega H_{rms}}{\sinh(kd)} \right)^3 \qquad (7)$$

where H_{rms} is the rms value of wave height. The energy loss factor f_e is a function of the Nikuradse roughness parameter, k_N.

The other calibration factor are the friction coefficients which are used in the model to specify the partial reflection from breakwaters or from the surrounding area (in our case it is the later). The simulations showed that there is a sensitivity in the variation of these friction coefficients which specify the reflections from the rocks surrounding the area of interest.

A series of simulations were performed. Wave breaking was included in all of the simulations. The energy dissipation due to wave breaking is calculated by the Battjes and Janssen formulation.

The program calculates the maximum wave height at all grid points. In Figure 5, contour plots of the maximum wave heights are shown. In this simulation spectral parameters recorded at the 100m buoy location at 03052317 (MMDDhhmm) were used as input to the model (Hs=3.65m,

Tp=9.09sec, θ=359 deg). The reflection coefficients which were used are 0.20, 0.10,0.25.

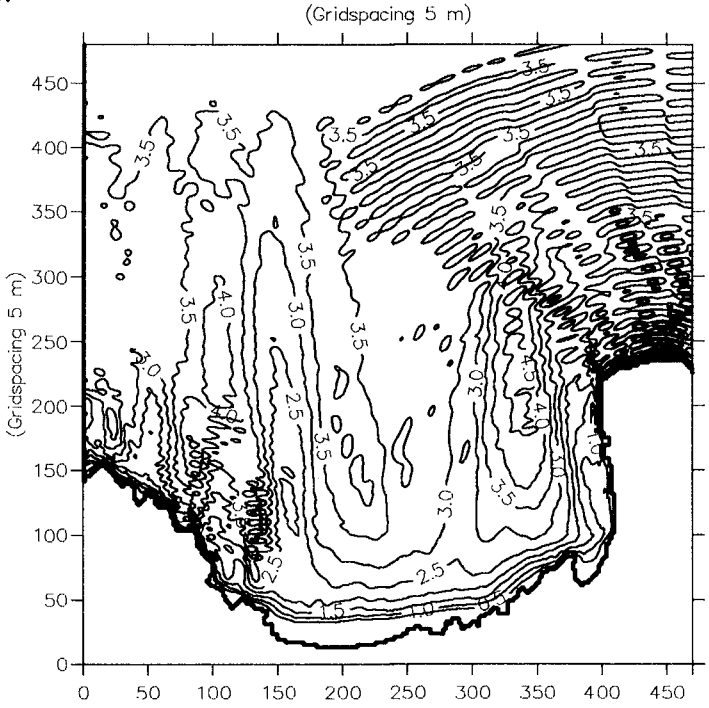

Figure 5. EMS simulation, contours of maxH, input H=3.65m, T=9.09sec, θ=359°.

Boussinesq Wave Model

This model is based on the numerical solution of the two-dimensional Boussinesq equations. These equations include non-linearity and frequency dispersion. In the classical form of the Boussinesq equations there is a very restrictive limitation on the maximum water depth in the simulation area (max $d/L_0 = 0.22$). In the new forms of the equations, which are used in DHI's MIKE21 BW model, this ratio can go up to $d/L_0=0.5$ (Madsen et al., 1991).

Most wave transformation processes are taken into acount in this model shoaling, refraction, diffraction and partial reflection from breakwaters and structures. Bed friction can also be included in the simulation. The only shortcoming of this model is wave breaking, which is not included in the energy dissipation processes. The basic equations, which are solved, are the continuity, the x -Momentum and the y - Momentum (Mike21 BW User Guide & Manual):

$$nS_t + P_x + Q_y = 0 \qquad (8)$$

$$nP_t + \left(\frac{P^2}{h}\right)_x + \left(\frac{PQ}{h}\right)_y + n^2 g h S_x + n^2 P\left[\alpha + \beta\frac{\sqrt{P^2+Q^2}}{h}\right] + \frac{gP\sqrt{P^2+Q^2}}{C^2h^2} + n\Psi_1 = 0$$

$$nQ_t + \left(\frac{Q^2}{h}\right)_y + \left(\frac{PQ}{h}\right)_x + n^2 g h S_y + n^2 Q\left[\alpha + \beta\frac{\sqrt{P^2+Q^2}}{h}\right] + \frac{gQ\sqrt{P^2+Q^2}}{C^2h^2} + n\Psi_2 = 0$$

where S, P, Q are surface elevation, and flux density in x-direction and flux density in y-direction respectively; subscripts denote partial differentiation, h is total depth, resistance coeffs, porosity, etc are included, whereas the non-linear Boussinesq terms Ψ_1 and Ψ_2 are cross terms of derivatives of fluxes and elevation. The equations are solved by implicit finite difference techniques, with variables defined on a space staggered rectangular grid.

Due to restrictions which are imposed by the model, the bathymetry which is used in BW simulations is modified: by choosing as a minimum wave period (cut-off frequency of the spectrum) $T_{min} = 6.02\text{sec}$, the maximum depth which can be allowed in the modelled area (assumption $d/L_0=0.60$, including deep water correction terms) is d_{max} = 34 m, whereas with the given grid spacing $\Delta x = 5$ m and the assumption $L/\Delta x=7$, the minimum water depth d_{min} is 4 m. The time step Δt which is used in the simulations is chosen on the basis of the resolution and the *Courant* criteria and is set as $\Delta t = 0.18\text{sec}$.

Bed Resistance is included in the model by means of a uniform number for the whole area of simulation (Chezy number C). Sponge layers all along the coastline were introduced in the BW simulations, in order to compensate for the energy absorption due to wave breaking, which cannot be modelled here.

Storm cases from March and November were chosen to demonstrate BW modelling. As input to the models (boundary conditions) time series of flux densities generated from the spectra of the heave time series recorded at the deep water (100m) buoy were used. The spectra were truncated at $T_{min} = 6.02\text{sec}$ or $f_{cut} = 0.17Hz$.

The output of these simulations are time series of wave elevation at all grid points of the modelled area. Contours of the significant wave heights, calculated as the RMS of the elevation time series for the whole period of simulation can also be drawn. In Figure 6 contour maps of significant wave heights H_s are plotted for the case date= 03052317, H_s=3.65m, T_p=9.09sec.

Spectral Transformation Methods

Spectral transformation techniques which focus on saturation, shoaling and refraction processes are also assesed by means of utilising them for the transformation of wave spectra recorded at the offshore location (100m) and comparing the resulting shallow water spectra with the ones measured at the two inner locations, for corresponding instances. Two methods are used, the TMA spectrum and the spectral slicing and reconstruction.

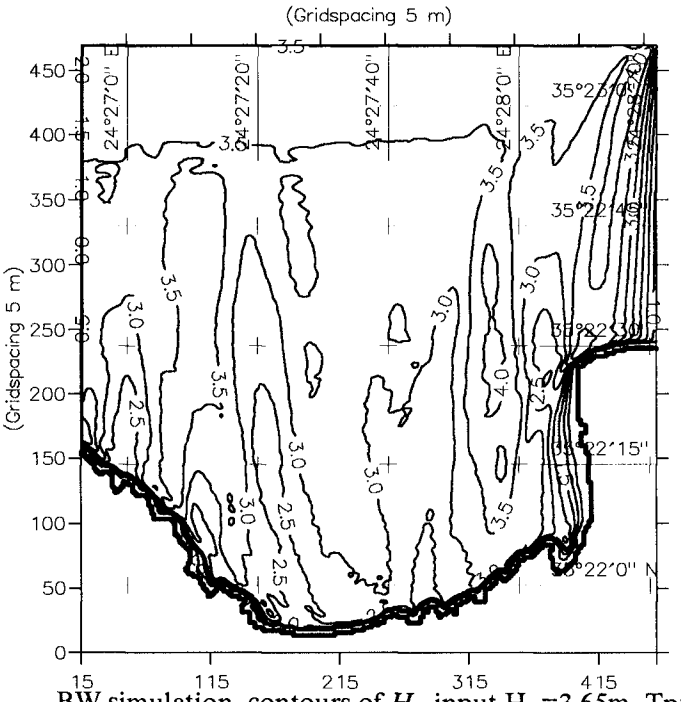

Figure 6. BW simulation, contours of H_s, input H_s =3.65m, Tp=9.09sec, θ=359⁰

TMA spectrum

The TMA spectrum yields an extension of the shelf-similar JONSWAP shape to finite water depth using the expression (Bouws et al., 1983)

$$E_{TMA}(f,H)=E_j(f)\,\Phi_\kappa(\omega_H) \tag{9}$$

where $E_j(f)$ is the well known JONSWAP spectrum and $\Phi_\kappa(\omega_H)$ is a transformation factor calculated through the relation

$$\Phi = tanh^2(kH)\{1+\frac{2kH}{sinh(2kH)}\}^{-1} \tag{10}$$

For a given spectrum, ie an output of the hindcast wave model or a measured spectrum at the offshore location, a JONSWAP spectrum with equivalent wave energy is estimated following the procedure, which is given in details elsewhere (Müller, 1976). Then the transformation factor for a specific depth is calculated and thus we obtain the TMA spectrum at a specific shallow site.

Spectral slicing and reconstruction

The incident wave energy spectrum, corresponding to a measurement at the outer location, is sliced to a number of discrete frequencies $f_1, f_2, \ldots\ldots, f_n$, so that the total incident wave energy is given as:

$$m_0 = \int_0^\infty S(f)df = \sum_{i=1}^{n} S(f_i)\Delta f_i = E_1 + E_2 + \ldots\ldots + E_n \qquad (11)$$

Each component is introduced to a linear numerical wave transformation model as a monochromatic wave with the frequency of this component. The relative wave height k_i or wave disturbance coefficient for every frequency f_i is calculated at every grid point in the studied area, and the resulting wave disturbance coefficient (of the pseudo-random wave) is consequently calculated by the formula:

$$k_{res} = \sqrt{\sum_{i=1}^{n} a_i k_i^2} \qquad (12)$$

where $\alpha_i = E_i/m_o$ is the percentage of wave energy which belongs to this particular discrete frequency f_i. The coefficents k_i are weighted either by the percentage of the total wave energy on this frequency (Equal Frequency method), or by the width of the frequency band it represents (Equal Energy), and then are superimposed.

Finally, the whole spectrum at a particular location ***P*** in the shallow area can be reconstructed, using the relation:

$$S(f_i, p) = |H(f_i, p)|^2 S(f_i) = k^2{}_{pi} \cdot S(f_i) \text{ or } \qquad S(f_i, p) = \frac{E_i}{df_i} k^2{}_{pi} \qquad (13)$$

where k_{pi} is the disturbance coefficient for component frequency i. In Figure 7 comparisons are shown between a measured spectrum in shallow water, a reconstructed with the equal frequency slicing method spectrum, and a TMA spectrum. We can observe that for the 20m location the agreement is good, although the slicing method cannot reconstruct the tail of the spectrum (which is expected since only a limited number of frequencies were included). At the 10m location, the TMA grossly underestimates the spectral peak

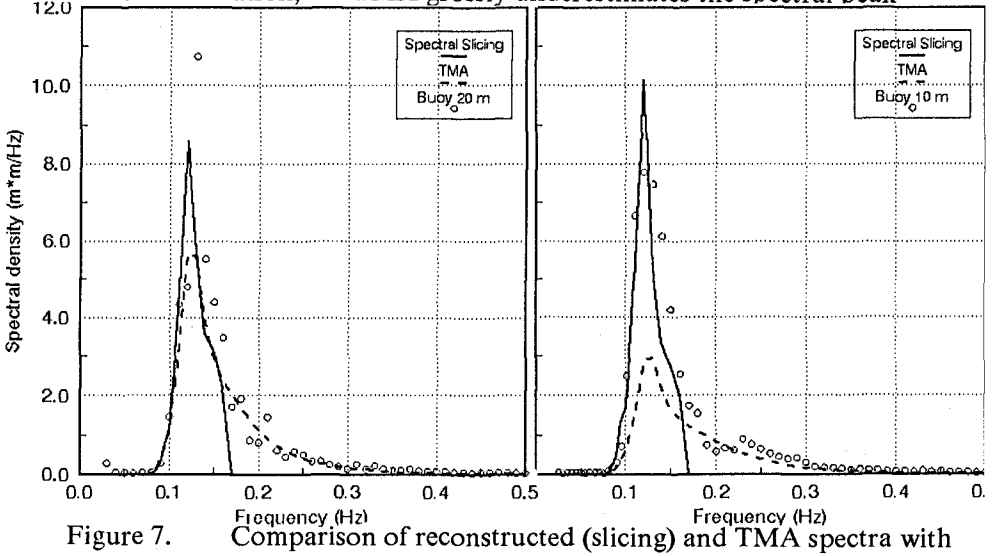

Figure 7. Comparison of reconstructed (slicing) and TMA spectra with measurements.

In Figure 8 the Hs calculated from the zero-th moment of the spectrum (slicing and reconstruction method) as $H_s=4*m_o^{1/2}$ is compared with the H_s of the measured spectrum, for a number of recordings in November 1994, for both the 20m and the 10m locations. We can see that the agreement is in general good, with some discrepancies appearing in the 10m location, since this approach cannot include non-linear wave dissipation effects.

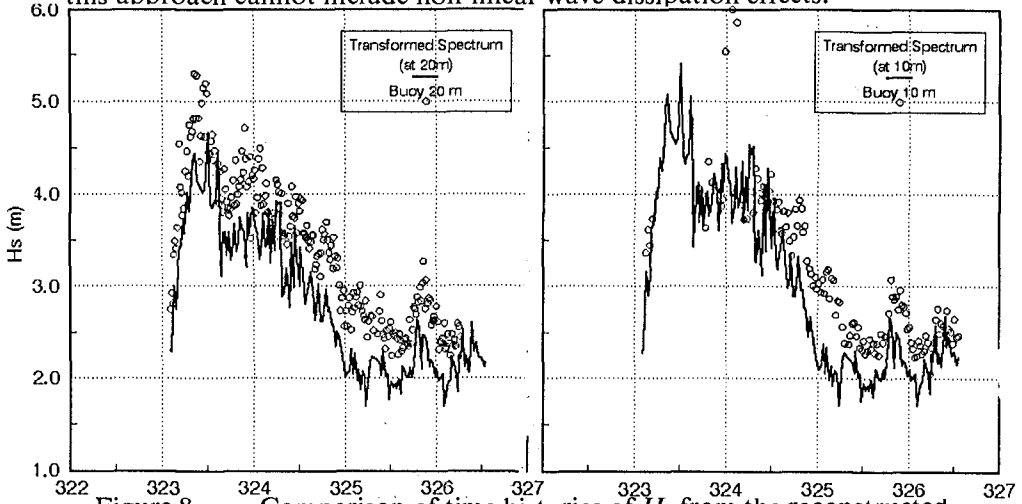

Figure 8. Comparison of time histories of H_s from the reconstructed (slicing) spectra with measurements.

Comparison of the methods

The methods which were employed in this work for the estimation of some of the nearshore wave climate parameters, are comparatively assessed in this section. In particular, the calculated wave heights, as they result from the numerical modelling are compared with the two inner buoys (20m and 10m) measured parameters. Transects, cutting perpendicularly to the coast are drawn on the contour maps of the solutions, whereas the corresponding measured parameters are marked on the same graphs.

In Figure 9 the case of date= 03052317, H_s=3.65m, T_p=9.09sec and θ=359 deg is presented; the results which are superimposed on the same graph are from the following simulations:

- EMS simulation with input parameters measured at the offshore location.
- BW simulation with input parameters measured at the offshore location.
- AUT shallow water simulation with input parameters calculated from the AUT hindcast model at the offshore location.
- BW simulation with input parameters calculated from the AUT hindcast model at the offshore location

It can be seen that wheras at the 20 m location most methods predict correctly the wave height, for the 10 m they overestimate it, which can be explained by the fact that they cannot include energy dissipation due to wave breaking. The BW simulation gives a better approximation, as it takes into account modal interactions. The SAUT model gives lower values overall due to initial underestimation at the offshore location.

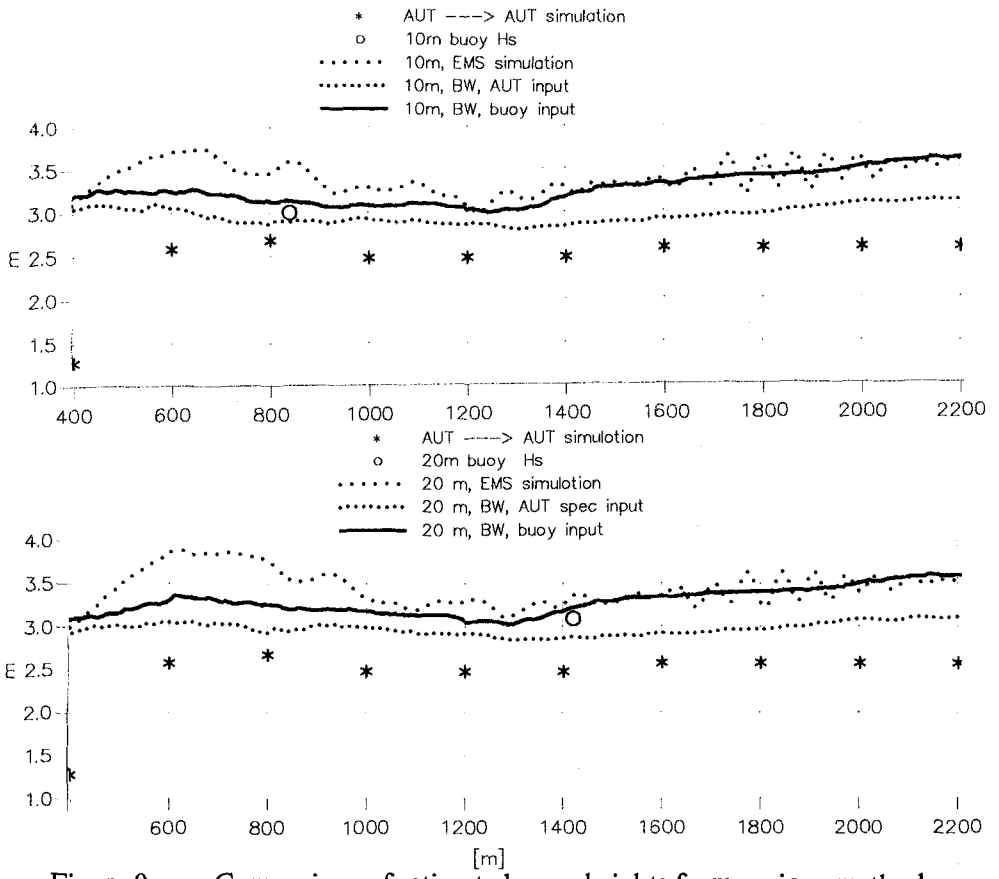

Figure 9. Comparison of estimated wave heights from various methods with measurements

In Figure 10 a comparison of the calculated disturbance coefficients for the case of date= 11201512, H_s=4.54m, T_p=9.09sec and θ=0 deg. is presented. The results which are superimposed on the same graph are from the following simulations:

- EMS simulation with input parameters measured at the offshore location.
- BW simulation with input parameters measured at the offshore location
- The Pseudo-random simulation (slicing and reconstruction)

It can be seen that whereas for the 20 m location the prediction is correct from all methods, for the 10m location the pseudo-random method is grossly overshooting, which can again be attributed to the ommision of both wave breaking and the interaction between modes.

Conclusions

Wave hindcast, numerical wave transformations and spectral transformation methods are employed for the assessment of the wave climate in a coastal area. The models are calibrated with the use of 10 month's duration of in situ wave measurements.

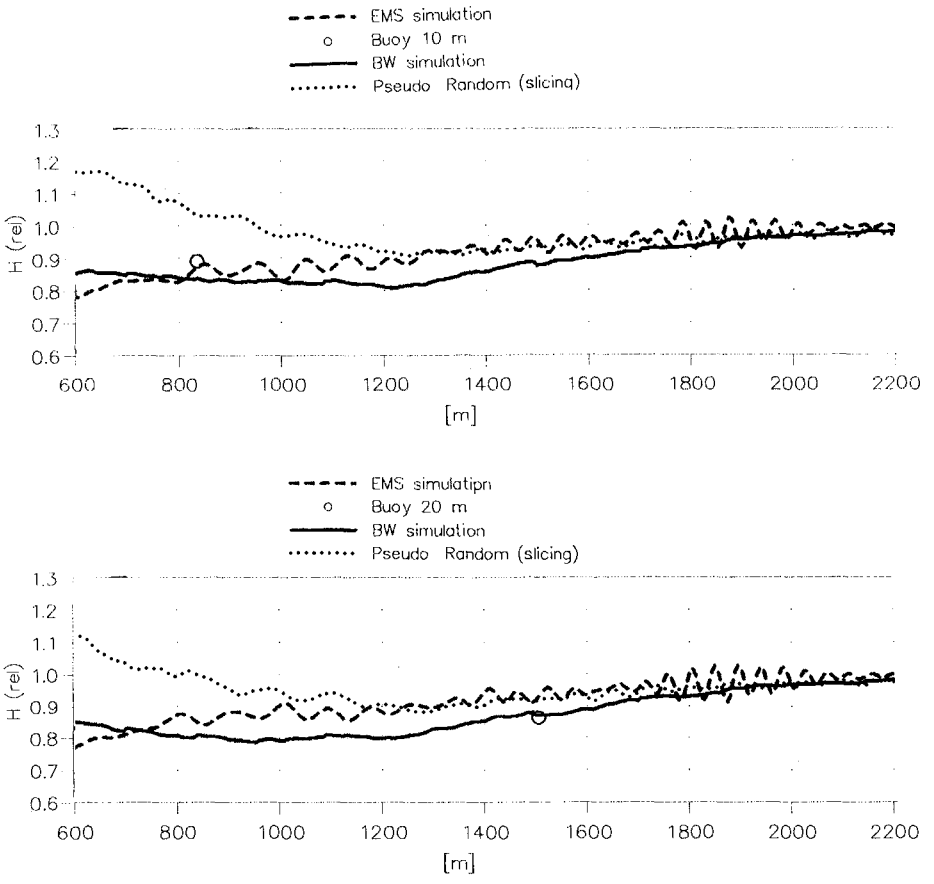

Figure 10. Comparison of estimated wave disturbance coeffs from various methods with measurements

The results of the deep water wave hindcast model compare well with the measured parameters. The results of the numerical wave transformation models match the measurements at the 20m and 10m buoys. It was found that, particularly for the monochromatic model (EMS), there is a sensitivity in the reflections from the area bordering the water. Despite the difference in scale (Δx and Δt) between the AUT shallow water model, and the BW and EMS models, they all predict correctly the wave parameters, as juxtaposed to the measurements.

Spectral transformation methods (TMA and slicing) seem to work well for the intermediate depth but not so well for the very shallow water. This is attributed to the lack of modelling both wave dissipation effects (breaking) and non-linear interactions. Great computational efficiency can be acheived though by using these methods.

Acknowledgements

The field campaign as well as part of the work of the second author has been carried out in the MAST II WAVEMOD project, in part funded by the EU contract no MAST2-CT92-0025. Part of the work of the first author was also funded by the MAST III SAFE project contract no. MAS3-CT95-0057.

References

Battjes J.A. and Janssen J.P.F.M., 1978.
Energy loss and set-up due to breaking of random waves, Proc. 16th ICCE, ASCE, pp. 569-588.

Berkhoff, J.C.W., 1976.
Mathematical Models for Simple Harmonic Linear Water Waves, Wave Diffraction and Refraction, Publication 163, Delft Hydraulics Laboratory, Delft, The Netherlands, pp 109.

Bouws E., Günther H., Rosenthal W. and Vincent C.L., 1985.
Similarity of the wind wave spectrum in finite depth water, 1. Spectral form, J. of Geoph. Research, 90, C1, pp. 975-996.

Christopoulos S. and Koutitas C., 1991.
Wave modelling in the North Aegean Sea, Ann. Geophysicae, 9, pp. 91-101.

Golding B.W., 1983.
A wave prediction system for real-time sea state forecasting, Quart. J. R. Met. Soc., 109, pp. 393-416.

Komen G.J., Hasselmann S. and Hasselmann K., 1984.
On the existence of a fully developed wind-sea spectrum, J. of Phys. Oceanography, 14, August, pp. 1271-1285.

Komen G.J., Cavaleri L., Donelan M., Hasselmann K., Hasselmann S. and Janssen P.A.E.M., 1994.
Dynamics and Modelling of Ocean Waves, Cambridge University Press, pp. 532.

Madsen P, Murray R. and Sorensen O., 1991.
A new form of the Boussinesq equations with impoved linear dispersion characteristics, Coastal Engineering, 15, pp. 371-368.

MIKE 21 EMS & BW Wave Modules, 1994.
User Guide and Reference Manuals, Rel. 2.4, DHI.

Müller P., 1976.
Parametrization of one-dimensional wind wave spectra and their dependence on the state of development, Heft 31, Hamburger Geophysikalische Einzelschriften, pp. 177.

Paillard M., 1995.
The Greek Field Experiment in the MAST 2- WAVEMOD- Project, IFREMER, MAST - WAVEMOD, TEC-1.3-02, March.

Solomonidis C., 1995.
Logistical Aspects of the Greek Site experiment, MARTEDEC, MAST - WAVEMOD Project, TEC -1.3 - 05, March.